

A-1-3

## High-Resolution Measurement of Ultra-Shallow Structures by Scanning Spreading Resistance Microscopy

Li Zhang<sup>1</sup>, Kazuya Ohuchi<sup>2</sup>, Kanna Adachi<sup>2</sup>, Mitsuhiro Tomita<sup>1</sup>, Kazunari Ishimaru<sup>2</sup>, Mariko Takayanagi<sup>2</sup> and Akira Nishiyama<sup>1</sup>

<sup>1</sup>Advanced LSI Technology Laboratory, Corporate Research & Development Center, Toshiba Corporation  
1, Komukai-Toshiba-cho, Saiwai-ku, Kawasaki 212-8582, Japan

<sup>2</sup>Center For Semiconductor Research & Development, Toshiba Corporation Semiconductor Company  
8 Shinsugita-cho, Isogo-ku, Yokohama, Kanagawa 235-8522, Japan  
Phone: +81-44-549-2192; E-mail: [Li.Zhang@toshiba.co.jp](mailto:Li.Zhang@toshiba.co.jp)

### 1. Introduction

To achieve high performance for ultra-shallow junction CMOSFETs, precise control of source/drain extension (SDE) and halo distributions is required [1-3]. Although SIMS is effective for accurate analysis of depth profile, a two-dimensional (2D) characterization method is limited mainly to scanning probe microscopy (SPM) [4,5]. Among the SPM technologies, scanning spreading resistance microscopy (SSRM) has been shown to be a promising method in view of its capability of direct conversion to 2D carrier-concentration distributions [4]. Recently, we obtained repeatable and high-resolution SSRM images by measuring in a vacuum [6] and confirmed reproducible depth profile for 10 nm-ultra-shallow junctions.

In this study, we estimate the spatial resolution of SSRM measurement by calibrating a standard sample with  $\delta$ -doped ultra-shallow layers and confirmed a sub-5 nm spatial resolution. The millisecond annealed CMOSFETs were also characterized and a difference of 2D halo distributions is observed between pMOS and nMOS devices, which is in good agreement with SIMS results.

### 2. Experimental

Figure 1 shows a schematic circuit of an SSRM in vacuum. Cross-sectional samples are prepared for 2D measurement. Commercially available diamond-coated Si probes are used for SSRM and the bias is applied to the sample back end. Measurements were performed in an AFM chamber in vacuum ( $< 1 \times 10^{-5}$  Torr) to prevent anode oxidation and to eliminate the contamination layer on the sample surface, as well as to prevent quick wearing out of the probes.

A standard sample with  $\delta$ -doped-boron-layers on Si substrate was used for depth calibration and for estimation of carrier activation status. Multi- $\delta$ -doped layers were prepared by MBE growth with spacing of  $5 \pm 0.2$  nm and  $20 \pm 0.2$  nm, respectively. As grown  $\delta$ -doped sample without additional thermal treatment was used for both SSRM and SIMS measurements. Millisecond annealed pMOSFETs and nMOSFETs were also used for measurement.

### 3. Results and discussion

Figure 2 shows (a) an SSRM image of the multi- $\delta$ -doped layers and (b) the TEM image of the same sample. From Fig. 2(a), the multi- $\delta$ -doped boron layers show bright contrast against the surrounding Si substrate, indicating that the  $\delta$  layers are conductive. The top three  $\delta$  layers of 5 nm spacing are successfully resolved, which means a sub-5 nm spatial resolution is achieved. Comparison of the depth scales between Figs. 2(a) and (b) also shows that the spacing of the multi-layer in the SSRM image agrees well with that of the TEM results. These results show that the SSRM measurement has sufficiently high resolution and is sufficiently ac-

curate for shallow layer analysis.

Next, we compared the depth profiles of SSRM and SIMS results as shown in Figs. 3(a) and (b), respectively. In Fig. 3(a), the top three layers of 5 nm spacing and the following 4 layers of 20 nm spacing can be recognized clearly. Because the SSRM current is proportional to the carrier concentration, we can compare the SSRM dynamic range directly with SIMS results. From Fig. 3, there is a nearly four-order change in the peak to valley SIMS concentrations for the 20 nm-spacing layers. The SSRM result shows a two-order change on the same layers. It should be noted that SIMS reflects the whole amount of boron atoms, whereas SSRM reflects the amount of the activated carrier portion of boron atoms. Considering the highest concentration is more than  $8 \times 10^{20} \text{ cm}^{-3}$ , the difference of the concentration range may be attributable to the inactivated part of boron atoms. This indicates the possibility of using SSRM to calibrate the activation ratio of carriers in ultra-shallow doping layers.

SSRM images of pMOS and nMOS FETs are shown in Figs. 4(a) and (b) and their contour maps in Figs. 4(c) and (d), respectively. From Fig. 4, the regions of the device structure are clearly distinguished in both pMOS and nMOS, including the halo regions, whose distributions have an important bearing on the device performance. A difference is found in that the halo region of nMOS is located far from the SDE junction compared with the halo of pMOS, as indicated by the profiles shown in Fig. 5. This result is in good agreement with SIMS results reported previously [3], as shown in Figs. 6(a) and (b). In addition, the SSRM 2D image shows that the halo of nMOS is located far from the SDE junction two dimensionally, which fact cannot be recognized in the case of SIMS results.

### 3. Conclusions

A sub-5nm spatial resolution was successfully achieved with precise SSRM measurement by calibrating a multi- $\delta$ -doped-layer sample. The halo-distribution difference in millisecond annealed ultra-shallow-junction pMOS and nMOS was also confirmed.

### Acknowledgements

The authors are grateful to N. Fukushima of Toshiba Corp. for encouragement to undertake this work.

### References

- [1] K. Adachi, *et al.*, *Symp. VLSI Tech. Dig.*, p. 142, (2005).
- [2] Y. Taur, *et al.*, *IEDM Tech. Dig.*, p. 789 (1998).
- [3] H. Tsujii, *et al.*, *IWJT Proc.*, p. 107, (2005).
- [4] A. Alvarez, *et al.*, *Appl. Phys. Lett.* **82**, p. 1724, (2003).
- [5] H. Fukutome, *et al.*, *IEDM Tech. Dig.*, p. 894, (2005).
- [6] L. Zhang, *et al.*, *to be published in IWJT Proc.*, (2006).

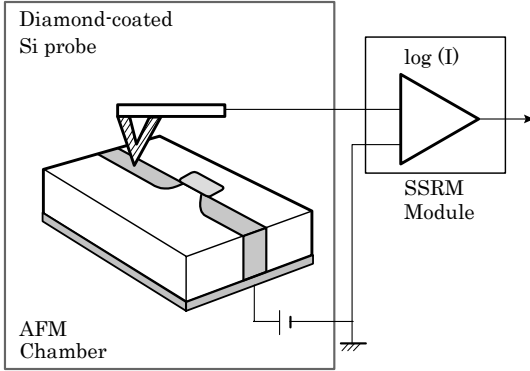


Fig. 1. Schematic circuit of SSRM in vacuum. Commercially available diamond-coated probes are used.

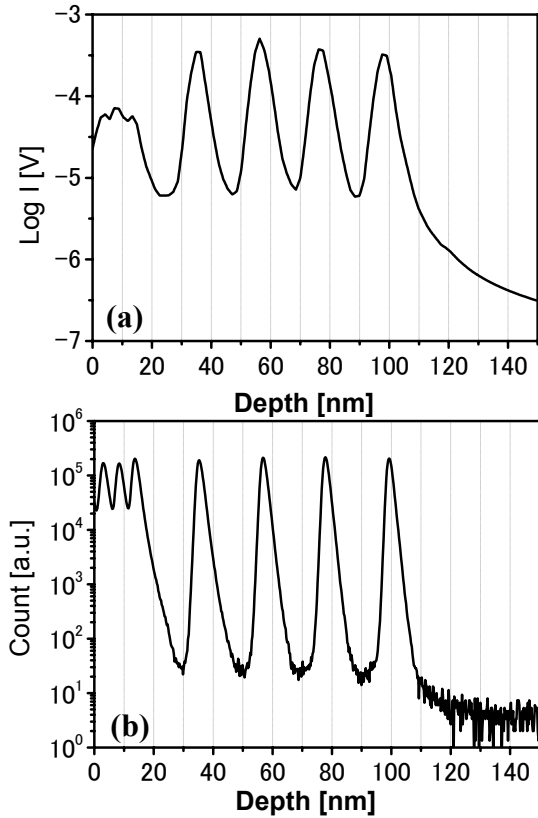


Fig. 3. (a) SSRM profiles along AA' of Fig. 2(a). (b) SIMS profiles of the same  $\delta$ -doped layers.

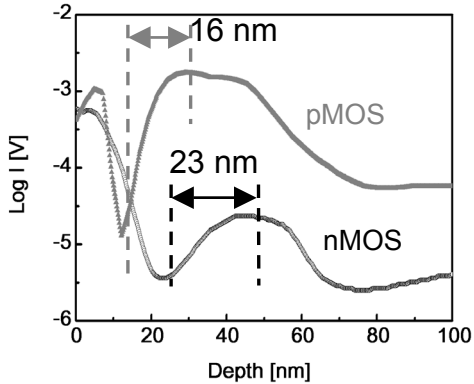


Fig. 5. SSRM profiles along BB' of Fig. 4(a) and CC' of Fig. 4(b).

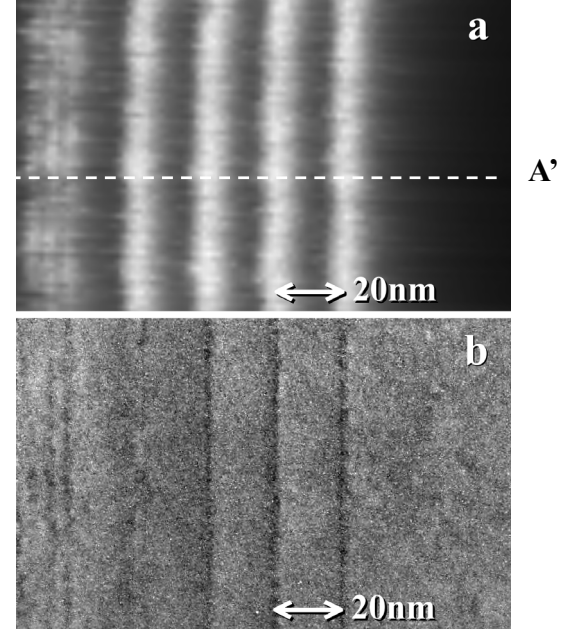


Fig. 2. (a) SSRM image of the multi- $\delta$ -doped layers. (b) TEM image of the same  $\delta$ -doped layers.

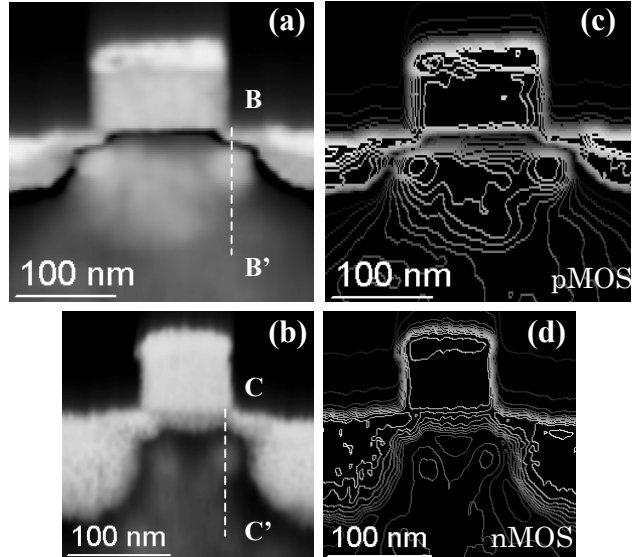


Fig. 4. SSRM images of (a) pMOS and (b) nMOS and their contour-mapping images (c) and (d), respectively.

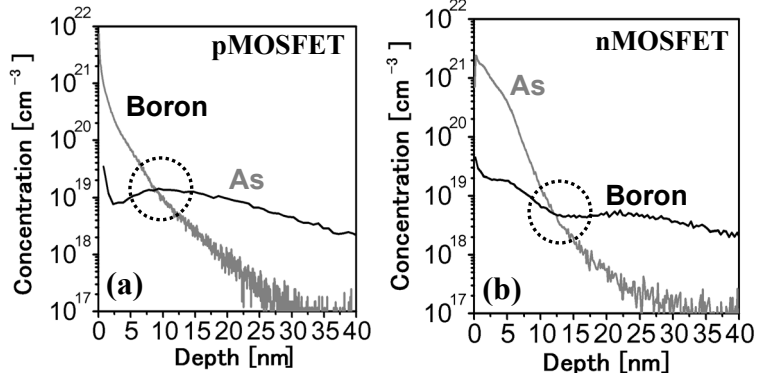


Fig. 6. SIMS profiles of boron and As in (a) pMOS and (b) nMOS, respectively.